Robust Haptic Teleoperation of a Mobile Manipulation Platform

Jaeheung Park and Oussama Khatib

Stanford AI Laboratory
Stanford University
http://robotics.stanford.edu

Abstract. This paper presents a new teleoperation scheme for mobile manipulation systems. A virtual spring connects a master and slave system where local force feedback on the slave system compensates for the dynamics of the mobile manipulator. This scheme is robust in the presence of time delays and disturbances and provides good tele-presence. The slave manipulator is mounted on a mobile base and controlled within the operational space framework. In this framework, the redundancy of the mobile manipulation system is addressed through a decoupled decomposition of task and posture dynamics.

1 Introduction

Tele-manipulation provides telepresence by allowing a user to remotely control a slave robot through a master device. These systems offer great potential, however, connecting master/slave stations in a coherent way is a challenging task. While the master station is controlled by the human operator, the slave station often interacts with an unknown and dynamic environment. The nature of such interaction greatly influences overall system performance.

Many teleoperation schemes have been developed to improve telepresence and stability when position and force measurements are available on both the master and slave [7,8,6]. Most of these schemes provide direct contact force feedback to the user for a greater level of telepresence. However, this feedback degrades the stability of the overall system especially if the mass properties of the master and slave differ significantly [3]. This paper proposes a new teleoperation scheme that utilizes local force control while exchanging position information between the master and slave station. Such an approach provides much better stability characteristics, while offering the user a realistic feeling of telepresence through the use of a virtual spring. This architecture is especially suited for systems where force sensing is limited to the slave robot and when the master device is relatively light and frictionless. Specifically, our setup which uses a Phantom device and PUMA mounted on a mobile base meets this criteria.

The operational space formulation [5] decouples the dynamics of the mobile manipulator into end-effector task dynamics and posture dynamics. Furthermore, each end-effector DOF can be independently controlled. The control of the base can be separately synthesized since its dynamics are decoupled from that of the end-effector. Based on this formulation, our new teleoperation scheme is applied for each end-effector DOF.

To deal with uncertainties and time-varying parameters (e.g. dynamic environments), the force control on the slave robot uses Active Observers (AOBs) [1], which modify the Kalman estimation structure to achieve model-reference adaptive control. In this case, the stiffness parameter has to be identified on-line to improve robustness and telepresence. The AOB is designed to cover a medium range of stiffness values. However, for large variations, on-line stiffness estimation is necessary [2]. Time delay associated with the wireless LAN network is also analyzed for our system.

2 Control for a Mobile Manipulator

The equations of motion for the end-effector of a robotic manipulator can be described using the operational space formulation [5],

$$\Lambda(q)\dot{\vartheta} + \mu(q,\dot{q}) + p(q) + F_c = F \tag{1}$$

where $\Lambda(q)$, $\mu(q,\dot{q})$, and $p(q)$ are the inertia matrix, the vector of Coriolis/centripetal forces, and the gravity vector in operational space, respectively. The term ϑ denotes the instantaneous velocity in operational space coordinates. The term F_c is the contact force at the end-effector. The control torque is selected as,

$$\Gamma = J^T F + N^T \Gamma_0 \tag{2}$$

$$F = \hat{\Lambda} F^* + \hat{\mu} + \hat{p} + \hat{F}_c \tag{3}$$

where N^T is the dynamically consistent null space projection matrix and F^* is the command to the unit mass system. The $\hat{}$ indicates an estimate of a particular quantity. The following decoupled equations of motion for the end-effector are obtained.

$$\dot{\vartheta} = F^* \tag{4}$$

The command F^* is composed of force and motion control components that are projected by the selection matrices, Ω_f and Ω_m, respectively.

$$F^* = \Omega_f F_f^* + \Omega_m F_m^* \tag{5}$$

In the experimental setup, force control is used to control only the Cartesian position of the end-effector since the master device does not provide force feedback on the orientation. The selection matrices are

$$\Omega_f = \begin{bmatrix} I_3 & 0_3 \\ 0_3 & 0_3 \end{bmatrix}, \qquad \Omega_m = \begin{bmatrix} 0_3 & 0_3 \\ 0_3 & I_3 \end{bmatrix} \tag{6}$$

where I_3 is the 3×3 identity matrix and 0_3 is the 3×3 zero matrix.

The control of the mobile base is applied to Γ_0 in Equation (2). The dynamically consistent null space projection matrix N^T prevents control of the mobile base from affecting the end-effector control.

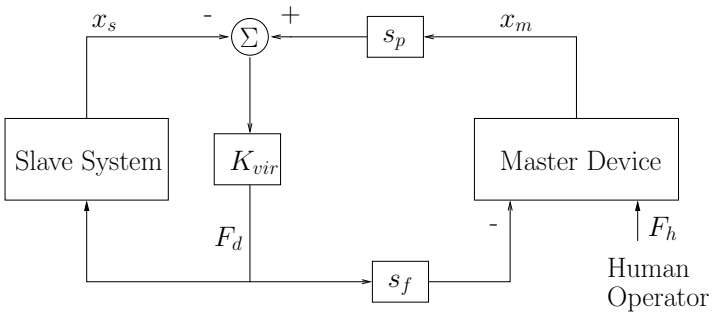

Fig. 1. Teleoperation Scheme. x_m, x_s, s_p and s_f are the master position, slave position, position scaling and force scaling, respectively. s_p and s_f are 2.0 and 0.1 in the experimental setup. K_{vir} is the virtual spring that generates the desired force, F_d.

3 Teleoperation

The teleoperation scheme is developed for each direction in operational space coordinates (i.e. one DOF system) since the control structure in Section 2 enables each Cartesian direction of a manipulator end-effector to be controlled independently. Figure 1 illustrates the proposed teleoperation scheme. The proposed scheme is simply to connect the master and slave system with a virtual spring. Then, force control is used on the slave manipulator to eliminate the dynamics of the slave robot.

The desired force, F_d, for both master and slave systems is generated by the virtual spring K_{vir} due to the position error. The contact force on the slave end-effector is controlled to track the desired force, F_d. The force controller in the slave system is implemented using a modified Kalman Estimator with full state feedback(AOB). However, only feedforward control is used to generate the desired force on the master side since the device is light weight and has low friction.

Stability characteristics of the system are improved by providing the desired contact force to the operator rather than the measured contact force. The direct use of the measured contact force causes a delay in the loop and the stability of the system is greatly dependent upon the mass ratio of the master and slave systems [3].

3.1 Telepresence

The user is always provided with the contact force that is scaled by s_f through a haptic device if the force control in the slave robot tracks the desired contact force well. Moreover, the transfer function, $\frac{X_m(s)}{F_h(s)}$, from the force of a human operator to the master position represents the compliance that the human operator feels at the master device [7]. Telepresence would be realized if the transfer function closely matches the slave system compliance.

In Figure 1, the master device is modeled with a mass and damper system, having the transfer function of $1/(m_m s^2 + c_m s)$. The slave system represents the

force controlled robot in contact with environment; thus, the transfer function from the desired force to the slave position, $\frac{X_s(s)}{F_d(s)}$ is represented by $G_{se}(s)$. The equations of motion for the master and slave are

$$(m_m s^2 + c_m s)X_m(s) = F_h(s) - s_f K_{vir}(s_p X_m(s) - X_s(s)) \quad (7)$$

$$G_{se}(s)K_{vir}(s_p X_m(s) - X_s(s)) = X_s(s), \quad (8)$$

where $X_m(s)$ and $X_s(s)$ are the Laplace Transform of x_m and x_s. Moreover, the environment on contact is modeled to have a certain stiffness, K_s,

$$F_c = K_s x_s, \quad (9)$$

where F_c is the contact force with the environment. Therefore, $G_{se}(s)$ can be represented by

$$G_{se}(s) = \frac{X_s(s)}{F_d(s)} = \frac{1}{K_s}\frac{F_c(s)}{F_d(s)}. \quad (10)$$

$G_s(s) = \frac{F_c(s)}{F_d(s)}$ is the closed loop transfer function of the force control in the slave system; thus, $G_{se}(s) \approx \frac{1}{K_s}$ within the bandwidth of the force controller. With (7) and (8), the transfer function $\frac{X_m(s)}{F_h(s)}$ can be derived as

$$\frac{X_m(s)}{F_h(s)} = \frac{K_{vir}+G_{se}(s)^{-1}}{(m_m s^2+c_m s+K_{vir}s_p s_f)(K_{vir}+G_{se}(s)^{-1})-K_{vir}^2 s_p s_f}. \quad (11)$$

Equation (11) shows the characteristics of the proposed teleoperation scheme. If $K_{vir} \gg |G_{se}^{-1}|$, at a low frequency range, $|m_m s^2 + c_m s| \ll K_{vir}s_p s_f$, the compliance that a human operator feels will be close to the environment compliance, $\frac{X_m(s)}{F_h(s)} \approx \frac{1}{s_p s_f K_s}$. At a high frequency range, $|m_m s^2 + c_m s| \gg K_{vir}s_p s_f$, it will be $\frac{X_m(s)}{F_h(s)} \approx \frac{1}{m_m s^2+c_m s}$.

Therefore, the key aspect for telepresence is to maintain $K_{vir} \gg |G_{se}^{-1}|$, i.e. $K_{vir} \gg K_s$, in addition to having a large force control bandwidth. The value of K_{vir} is limited by the stability. To maintain the ratio $\frac{K_{vir}}{K_s}$ as large as possible within this limit, K_{vir} is updated on-line based upon the estimated environment stiffness. That is, K_{vir} is increased with the estimate of K_s. The following equation is used in the experiments.

$$K_{vir} = 2000.0\sigma_d(0.007(\hat{K}_s - 1000.0)) + 1000.0 \quad (12)$$

where $\sigma_d(x) = \frac{1}{1+e^{-x}}$.

3.2 Stability

The characteristic equation Δ of the loop is

$$\Delta = (m_m s^2 + c_m s)G_{se}(s)^{-1} + K_{vir}(m_m s^2 + c_m s + s_p s_f G_{se}(s)^{-1}). \quad (13)$$

The system is stable for any K_{vir} if the model is perfect because $G_{se}(s)$ is a stable minimum system with a constant DC value. However, the feedback gains K_{vir}

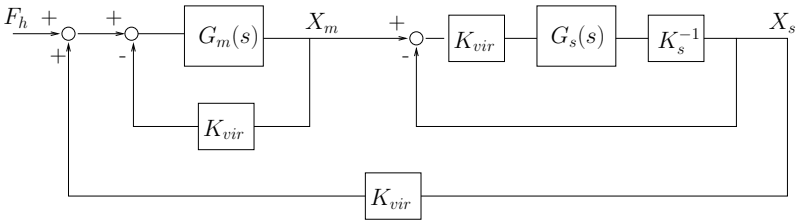

Fig. 2. Re-arranged block diagram. It highlights local feedback for each system in the proposed Teleoperation Scheme. $G_m(s)$ and $G_s(s)$ represent dynamics of the master device and the closed loop force control system of the slave manipulator. i.e. $G_m(s) = \frac{X_m(s)}{F(s)} = (m_m s^2 + c_m s)^{-1}$ and $G_s(s) = \frac{F_c(s)}{F_d(s)}$. X_m and X_s are the position of the master and slave system. F_h is the force from a human operator. F_c and F_d are the contact force and the desired contact force in the slave manipulator. K_s is the environment stiffness.

and K_{vir}/K_s are bounded by the physical limitations of the master device and the slave robot. Figure 2 shows the local feedback systems at the master and slave. Specifically, K_{vir} cannot exceed the maximum stiffness that the master device can produce. Also, $\frac{K_{vir}}{K_s}$ is limited by the motion bandwidth of the slave manipulator. In free space motion, where K_s is small, this results in greater limitation on the magnitude of K_{vir}.

3.3 Time delay

In the presence of time delay Equations (7) and (8) become

$$(m_m s^2 + c_m s)X_m(s) = F_h(s) - s_f K_{vir}(s_p X_m(s) - X_s(s)e^{-T_d s}) \quad (14)$$

$$G_{se}(s)K_{vir}(s_p X_m(s)e^{-T_d s} - X_s(s)) = X_s(s) \quad (15)$$

Now, the transfer function from the force of the human operator to the position of the master device is

$$\frac{X_m(s)}{F_h(s)} = \frac{K_{vir} + G_{se}^{-1}}{(m_m s^2 + c_m s + K_{vir} s_p s_f)(K_{vir} + G_{se}^{-1}) - K_{vir}^2 s_p s_f e^{-2T_d s}} \quad (16)$$

The effect of time delay on the performance is investigated using Padé approximation for small time delay, $e^{-2T_d s} = \frac{1-T_d s}{1+T_d s}$.

$$\Big[\frac{F_h(s)}{X_m(s)}\Big]_{\text{w delay}} = \Big[\frac{F_h(s)}{X_m(s)}\Big]_{\text{w/o delay}} + \frac{K_{vir}^2 s_p s_f \frac{2T_d s}{1+T_d s}}{K_{vir} + G_{se}(s)^{-1}} \quad (17)$$

The additional term, $\frac{K_{vir}^2 s_p s_f \frac{2T_d s}{1+T_d s}}{K_{vir}+G_{se}(s)^{-1}}$, can be further approximated as $2sT_d K_{vir} s_p s_f$ at a low frequency range when $K_{vir} \gg |G_{se}^{-1}|$. This shows the damping effect of the time delay. Stability is no longer guaranteed for large T_d.

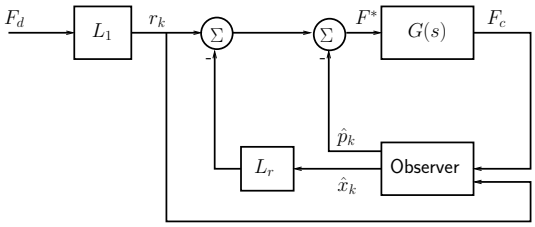

Fig. 3. Force Control Design. $G(s)$ is the system transfer function from the command F^* to the contact force F_c. F_d is the desired contact force. r_k, $\hat{x}_k$, and $\hat{p}_k$ are reference input, state estimate, and input error estimate. L_r and L_1 are a full state feedback gain and a scaling factor to compute reference input r_k.

4 Force Control

The decoupled unit mass system for each Cartesian direction (4) is used for force controller design. With the contact model (9), the equations of motion of contact force for each direction in operational space are,

$$\ddot{F}_c = K_s F^* \tag{18}$$

The system transfer function for contact force control is derived from a decoupled sub-system (18). With an additional damping, $K_v\vartheta$, to F^* for better stability and a system input delay, $T_{input,d}$, the overall system can be approximated by

$$G(s) = \frac{K_s e^{-sT_{input,d}}}{s(s + K_v)}, \tag{19}$$

where K_v is a positive scalar. The discretized state space form of Equation (19) is used for discrete Kalman estimation and control.

The overall force control scheme is illustrated in Figure 3. The AOB uses a probabilistic approach to estimate the states and input error. The estimated input error is directly compensated at the input command. A full state feedback is applied with the estimated states. More details on the implementation and robustness analysis can be found in [2].

4.1 Stiffness Adaptation

The slave manipulator in teleoperation experiences contact with different environments. The knowledge of the stiffness, K_s, is important not only for the force control but also for modifying the virtual spring, K_{vir}, to provide better telepresence to an operator. The changes can be abrupt and large in magnitude; thus, a fast on-line stiffness estimation strategy is required to cope with these changes.

The performance of force control without adaptation degrades in the presence of a large mismatch of the environment stiffness, as shown in Figure 4. Also, the different relationships between the desired, measured, and estimated contact force (F_d, F_m,

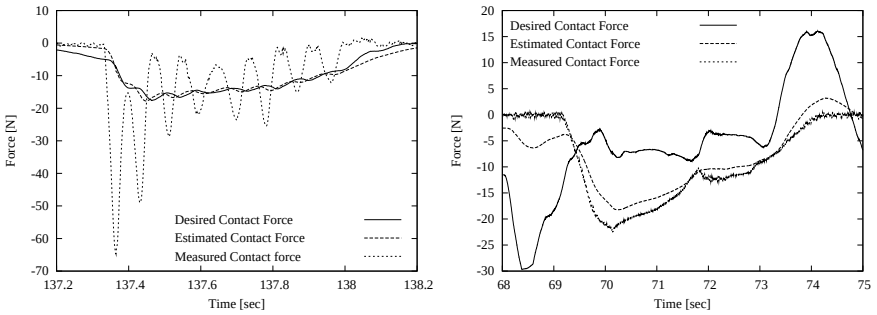

(a) (b)

Fig. 4. The results of force control without adaptation. (a) Nominal stiffness, $\hat{K}_s$, is 100 [N/m] and K_s changes from free space to 3000 [N/m]. (b) Nominal stiffness, $\hat{K}_s$ is 3000 [N/m] and K_s changes from free space to 300 [N/m].

and F_e) in Figure 4(a) and (b) are noticeable. In Figure 4(a), where $K_s \gg \hat{K}_s$, the difference between F_m and F_e is large while the difference between F_d and F_e is relatively small since the system response starts fluctuating (i.e., F_m oscillates around F_e). In Figure 4(b), where $K_s \ll \hat{K}_s$, the difference between F_d and F_e is larger than between F_m and F_e since the system response is sluggish.

In addition, it is observed that as the larger contact force is applied, the system stiffness increases. With these observations from the experiments, an adaptation law has been proposed [4]. This adaptation law combines the aforementioned two ideas; thus, it has two parts.

$$\hat{K}_s^i = \hat{K}_{s,1}^{f,i} + \hat{K}_{s,2}^{f,i}. \tag{20}$$

where the superscript i indicates the discrete time step and the superscript f indicates the filtered value. The first part of the estimation is based upon the relation between F_d, F_m, and F_e.

$$\hat{K}_{s,1}^i = \hat{K}_{s,1}^{i-1} + \Delta\hat{K}_{s,1}^i, \tag{21}$$

where $\Delta\hat{K}_{s,1}^i = k_1|F_m - F_e|\,\sigma_d\left(c, \frac{|F_m-F_e|}{|F_e|+a_1} - b_1\right) - k_2|F_d - F_e|\,\sigma_d\left(c, \frac{|F_d-F_e|}{|F_e|+a_2} - b_2\right)$, and $\sigma_d(c,x) = \frac{1}{1+e^{-cx}}$. The terms $k_1, k_2, a_1, a_2, b_1, b_2$ and c are positive parameters. The minimum of $\hat{K}_{s,1}$ is kept to 0.0 [N/m]. The second part of the estimation law (20) is based on the fact that the stiffness increases with the applied force.

$$\hat{K}_{s,2} = K_{min} + k_3\,\sigma_d\left(c_0, |F_m| - F_0\right), \tag{22}$$

where F_0, c_0 and k_3 are positive parameters. K_{min} is set to 100.0 [N/m] in the experiments. Finally, low-pass filters are used to prevent jerking motions due to quick changes in the stiffness estimation. All the parameters are obtained experimentally: a_1, a_2, b_1, b_2, c, and c_0 are 1.0, 0.1, 1.5, 1.0, 5.0, and 0.2 respectively. F_0, k_1, k_2, and k_3 are 20.0 N, 10.0 m^{-1}, 10.0 m^{-1}, and 3000.0 N/m.

5 Experimental Setup

(a) (b)

Fig. 5. System Setup. (a) Phantom^{TM} device controlled by a human. (b) PUMA robot mounted on XR4000 (ROMEO)

The slave station consists of a PUMA560 manipulator mounted on an XR4000 mobile base. The master station is a Phantom haptic device. Only position of the end-effector is controlled by teleoperation through force control. The end-effector rotation is simply controlled to maintain a fixed orientation. The XR4000 mobile base is controlled to track a trajectory autonomously in the null space. The time delay associated with the current wireless LAN setup is approximately 26 ms in each direction.

6 Results

Two sets of experiments were conducted to show the decoupling of the end-effector control from the base control. Only the PUMA robot was controlled through teleoperation in the first set of experiments. The results are shown in Figure 6-8. The second set of experiments was conducted while the base was also controlled to move in the lateral direction (i.e. along the table in Figure 5) using the null space control. The desired trajectory was a sine function with an amplitude of 20 cm and a period of 12 seconds as shown in Figure 9. The results are shown in Figure 10-12. The fact that there is little difference in the performance of the two sets of experiments demonstrates the effectiveness of the decoupled control structure.

In both experiments, the operator began moving the slave manipulator in free space (i.e. no contact) by teleoperation. The different objects were then contacted sequentially by the end-effector of the slave manipulator: a sponge, a book, and a table. Their stiffnesses were identified off-line as 300, 3000, and 6000 [N/m] respectively, in order to be compared with the estimated values in Figure 7(a) and Figure 11(a). The robot was in free space in between the contacts (i.e. where $F_m \approx 0$).

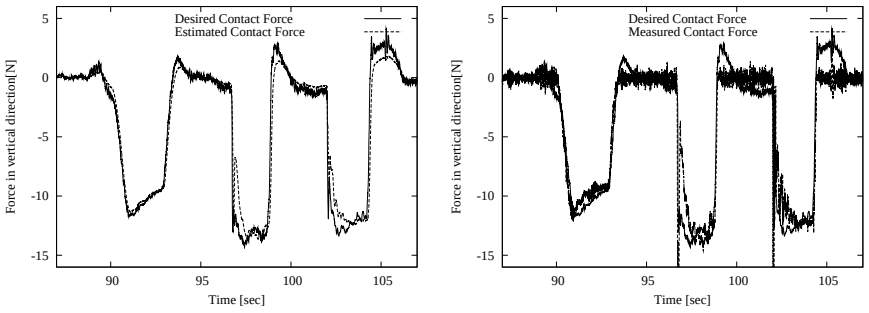

(a) (b)

Fig. 6. Fixed base teleoperation: force response. The desired, estimated, and measured force at the end-effector of the slave manipulator are compared in (a) and (b). The desired force is generated by a virtual spring, $K_{vir}(x_m - x_s)$. The estimated force is from the AOB (a modifi ed Kalman Estimator). The force is measured by the JR3 wrist force sensor.

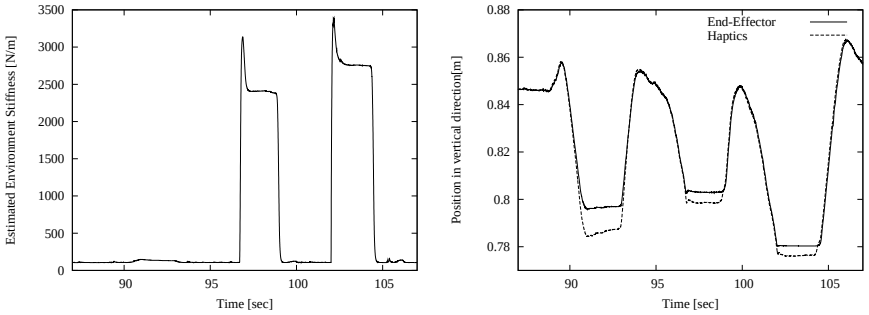

(a) (b)

Fig. 7. Fixed base teleoperation: $\hat{K}_s$ and position tracking. (a) The estimated stiffness $\hat{K}_s$ for the environment that the end-effector of the slave manipulator is in contact with. (b) The end-effector of the slave manipulator tracking haptic position in the vertical direction.

Figure 6 and 10 show the contact force in the vertical direction at the end-effector of the slave manipulator. The manipulator was in free space in the region where the measured contact forces were near zero. These results demonstrate that the force controller with AOBs and stiffness adaptation performs well even in the presence of vastly different environmental changes. The estimated environment stiffness $\hat{K}_s$ was updated quickly and accurately enough to achieve the designed performance and stability criteria as shown in Figure 7(a) and 11(a). Position tracking performance is shown in Figure 7(b) and 11(b).

The desired contact force for the slave end-effector and the applied haptic force are compared in Figure 8(a) and 12(a). Without time-delay, they would be exactly the same. However, the effect of time-delay results in large differences especially

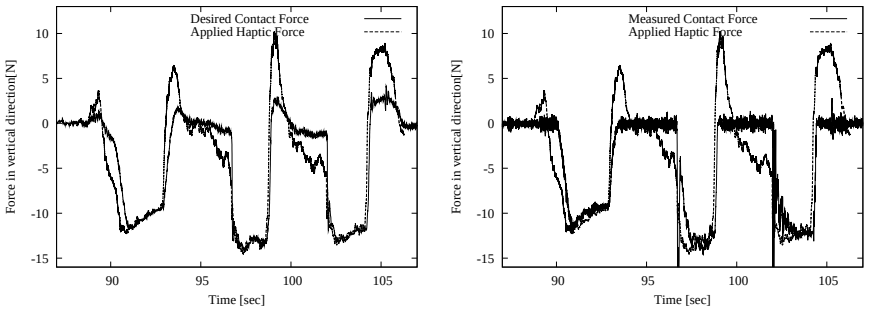

(a) (b)

Fig. 8. Fixed base teleoperation: force comparison at the slave and master.(a) The haptic force and the desired contact force. The difference between them comes from the effect of time-delay. The haptic force is multiplied by the scaling factor 10.0 for comparison. (b) The haptic force and the measured contact force.

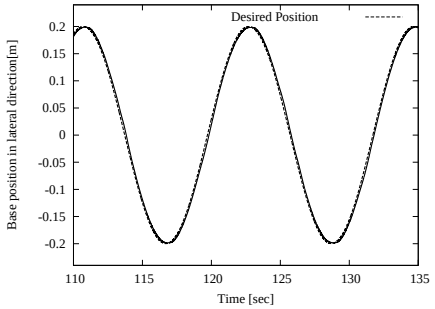

Fig. 9. Moving base teleoperation: base motion. The base moves in the lateral direction, (i.e. along the table in Figure 5) while the end-effector of the slave manipulator is controlled by teleoperation. The amplitude is 20 cm and the period is 12 seconds.

in free space motion. This contributes to the damping effect that the operator feels in free space operation. Figure 8(b) and 12(b) illustrates the measured contact force with the applied haptic force to the operator.

7 Conclusion

Robust local force control enables the overall teleoperation scheme to be simple and stable while providing realistic force feedback to a human operator. There is no switching in the control structure for different environments. The on-line stiffness adaptation performs effectively enough to match the changes in the environment. Thus, the entire tele-manipulation is always stable within the time delay margin. The teleoperation scheme developed for a single DOF system has been successfully

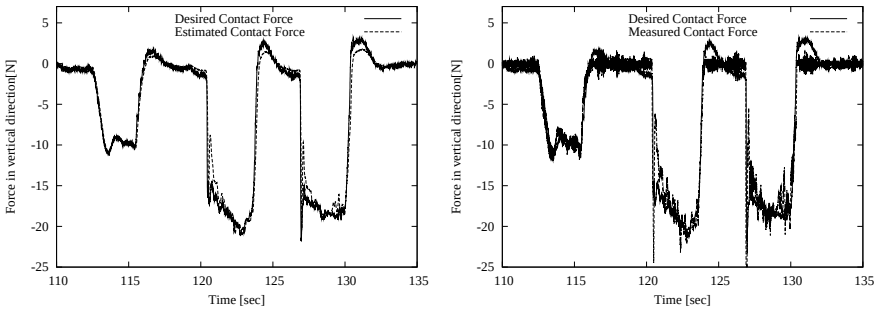

(a) (b)

Fig. 10. Moving base teleoperation: force response. The desired, estimated, and measured force at the end-effector of the slave manipulator are compared in (a) and (b). The desired force is generated by a virtual spring, $K_{vir}(x_m - x_s)$. The estimated force is from the AOB (a modifi ed Kalman Estimator). The force is measured by the JR3 wrist force sensor.

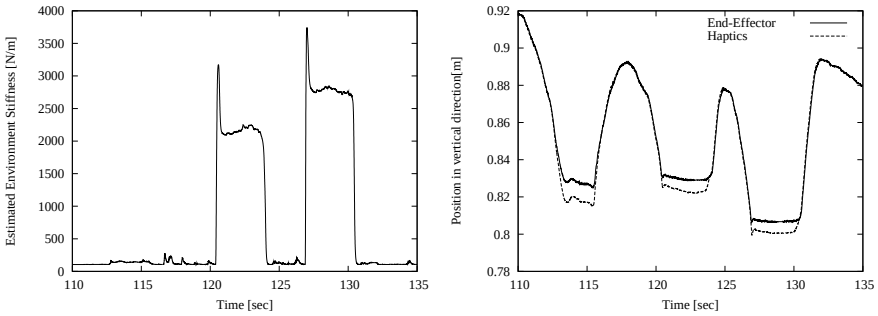

(a) (b)

Fig. 11. Moving base teleoperation: $\hat{K}_s$ and position tracking. (a) The estimated stiffness $\hat{K}_s$ for the environment that the end-effector of the slave manipulator is in contact with. (b) The end-effector of the slave manipulator tracking haptic position in the vertical direction.

applied to the mobile manipulator using the operational space framework. The user is able to control the end-effector and feel the environment realistically while the mobile base autonomously achieves the specified goals.

Acknowledgment

The authors would like to acknowledge Peter Thaulad for his contributions to the setup of hardware for the mobile base and the manipulator gripper.

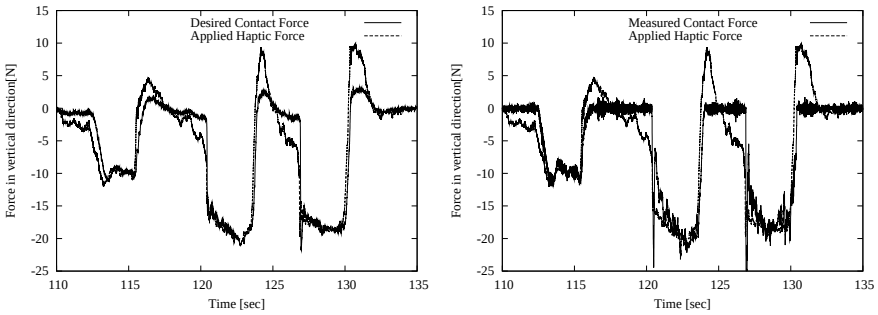

(a) (b)

Fig. 12. Moving base teleoperation: force comparison at the slave and master. (a) The haptic force and the desired contact force. The difference between them comes from the effect of time-delay. The haptic force is multiplied by the scaling factor 10.0 for comparison. (b) The haptic force and the measured contact force.

References

1. R. Cortesão. *Kalman Techniques for Intelligent Control Systems: Theory and Robotic Experiments*. PhD thesis, University of Coimbra, 2002.
2. R. Cortesão, J. Park, and O. Khatib. Real-time adaptive control for haptic manipulation with active observers. In *Proc. of the Int. Conf. on Intelligent Robots and Systems (IROS)*, pages 2938–2943, Las Vegas, 2003.
3. R. Daniel and P. McAree. Fundamental limits of performance for force reflecting teleoperation. *International Journal of Robotics Research*, 17(8):811–830, August 1998.
4. J.Park, R. Cortesão, and O. Khatib. Robust and adaptive teleoperation for compliant motion tasks. In *Proc. of the Int. Conf. on Advanced Robotics*, pages 513–519, Portugal, 2003.
5. O. Khatib. A unified approach for motion and force control of robot manipulators: The operational space formulation. *Int. J. on Robotics and Automation*, 3(1):43–53, February 1987.
6. W.S. Kim, B. Hannaford, and A.K. Bejczy. Force-reflecting and shared compliant control in operating telemanipulators with time delay. *Int. J. on Robotics and Automation*, 8:176–185, April 1992.
7. D. Lawrence. Stability and transparancy in bilateral teleoperation. *IEEE Trans. on Robotics and Automation*, 9(5):624–637, October 1993.
8. W. Zhu and S. Salcudean. Stability guaranteed teleoperation: An adaptive motion/force control approach. *IEEE Trans. on Automatic Control*, 45(11):1951–1969, November 2000.